HUMAN VACCINES & IMMUNOTHERAPEUTICS
2025, VOL. 21, NO. 1, 2479229
https://doi.org/10.1080/21645515.2025.2479229

Taylor & Francis
Taylor & Francis Group

RESEARCH ARTICLE

OPEN ACCESS Check for updates

Nanovaccine loaded with seno-antigen target senescent cells to improve metabolic disorders of adipose tissue and cardiac dysfunction

Kexin Zhang[a*], Qiliang Yin[a*], Yucen Ma[a], Mengyu Cao[a], Lingwei Li[a], Xinliang Jin[b], and Jiyan Leng[a]

[a]Department of Cadre Ward, The First Hospital of Jilin University, Changchun, China; [b]Department of General Surgery, First Affiliated Hospital of Changchun University of Traditional Chinese Medicine, Changchun, China

ABSTRACT

The buildup of senescent cells exacerbates metabolic disorders in adipose tissue and contributes to aging-related cardiac dysfunction. Targeted clearance of senescent cells can markedly ameliorate these aging-related diseases. Here, we developed a novel nanovaccine (GK-NaV) loaded with seno-antigen that is self-assembled from the fusion of cationic protein (K36) and seno-antigen peptide (Gpnmb). The GK-NaV could be highly engulfed by bone marrow-derived dendritic cells (BMDCs) and efficiently present antigens on the cellular surface, thereby promoting DCs maturation and activation of $CD8^+$T cells in vitro. Following subcutaneous immunization, GK-NaV not only exhibited a noticeable antigen depot effect but also markedly activated specific cellular immune responses, enhancing the immunoreactivity and cytotoxic effects of $CD8^+$T cells. Consequently, the targeted anti-aging immunity triggered by GK-NaV demonstrated the ability to selectively eliminate senescent adipocytes and cardiomyocytes in high-fat diet (HFD)-induced progeroid mice, leading to a significant improvement in age-related metabolic disorders in adipose tissue and cardiac dysfunction. Hence, our findings indicate that immunization with GK-NaV targeting seno-antigens may represent a promising strategy for novel senolytic therapies.

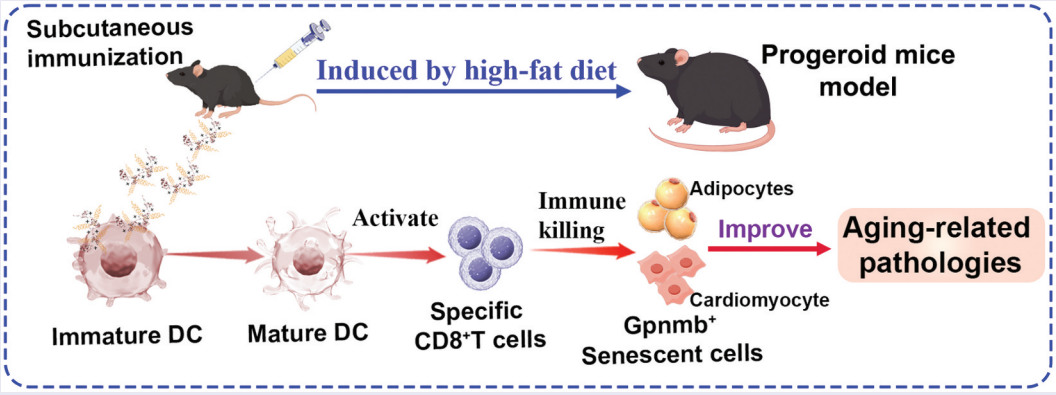

ARTICLE HISTORY
Received 3 January 2025
Revised 21 February 2025
Accepted 9 March 2025

KEYWORDS
Nanovaccine; seno-antigen; senescent cells; metabolic disorders; cardiac dysfunction

Introduction

Several lines of evidence suggest that as individuals age, senescent cells accumulate in various tissues and contribute to the progression of age-related disorders such as cancer, cardiovascular diseases, metabolic disorders, kidney diseases, and neurodegenerative conditions.[1–4] Prophylactic removal of senescent cells that express the senescence marker $p16^{INK4A}$ reduces tissue degeneration, delays tumorigenesis, and prolongs health span in mice, suggesting that these senescent cells contribute significantly to the aging process in organisms.[5,6] For instance, senescent cells gradually build up in the adipose tissue of aging mice, and the removal of these senescent cells from adipose tissue helps to mitigate the onset of metabolic abnormalities associated with aging.[7,8] Consequently, the elimination of senescent cells through senolysis or senolytic therapy offers an attractive anti-senescence therapeutic strategy for addressing aging-related pathologies. While several small molecules exhibit such activity, most are not sufficiently potent and lead to significant side effects.[9–11]

Under physiological circumstances, the immune system is capable of eliminating senescent cells.[12] The pro-inflammatory cytokines released by these cells attract and activate immune cells, resulting in their removal through immune-mediated processes.[12,13] Counterintuitively, senescent cells can build up in aging and disease states, evading removal by the immune system. This accumulation contributes to inflammation and

CONTACT Jiyan Leng lengjy@jlu.edu.cn Department of Cadre Ward, The First Hospital of Jilin University, 1 Xinmin Street, Changchun 130021, China.
*Kexin Zhang and Qiliang Yin contributed equally to this work.
Supplemental data for this article can be accessed online at https://doi.org/10.1080/21645515.2025.2479229

the progression of various diseases.[9,14] With the discovery of seno-antigen, vaccination targeting these antigens can elicit a specific anti-aging immune response and thus achieve the targeted clearance of senescent cells.[7,15,16] For example, to focus on particular subsets of senescent cells, Suda et al. employed an innovative strategy that first involved identifying a distinct biomarker (Gpnmb) for senescent endothelial cells, followed by the development of a peptide vaccine to selectively target these cells.[7] However, although peptide vaccines can induce specific immune responses against seno-antigenic epitopes, their immunogenic effects are somewhat limited due to factors such as poor stability and weak immunogenicity.[17,18] Thus, there is a need for an efficient vaccine delivery platform to enhance the immunogenicity of peptide antigens and to augment the specific immune effector responses.

Currently, nanovaccines incorporating antigen peptides have been created, offering distinct advantages over traditional whole organism-based vaccines to address antigen delivery challenges and stimulate targeted immune responses.[19–21] This approach has shown promise in the context of cancer and infectious diseases.[20–23] Nevertheless, little is known about the research on nanovaccines in the field of antisenescence. Herein, we constructed an innovative anti-aging nanovaccine (GK-NaV) by fusing cationic proteins (K36) with seno-antigen peptides (Gpnmb) and facilitating their self-assembly. GK-NaV forms stable, spherical nanoparticles that significantly stimulate the maturation of DCs (as evidenced by the upregulation of CD80 and CD86 expression) both in vitro and in vivo, and markedly activate $CD8^+$ T cells (immunological activity and immunological memory). In high-fat diet (HFD)-induced progeroid mice, it was observed that subcutaneous immunization effectively targeted and eliminated $Gpnmb^+$ senescent cells in adipose and cardiac tissues. This intervention remarkably ameliorated metabolic dysregulation in adipose tissue and cardiac dysfunction, thereby extending the lifespan of the progeroid mice.

Materials and methods

Gene expression and protein purification

K36 is an elastin-like protein with self-assembly capabilities. The plasmids encoding the K36 (pET25b-K36) were generously provided by Prof. HaoFan Jin. The Gpnmb gene, which encodes the Glycoprotein nonmetastatic melanoma protein B (sequences: AGGAGGGGAGACGGCAGGTGGAAGGAC), was synthesized by (GENEWIZ, The U.S.A), and the Gpnmb peptides (sequences: RRGDGRWKD) from mice were synthesized by Sangon Biotech Company (China). The plasmids encoding Gpnmb-K36 were constructed in our laboratory. In brief, the Gpnmb and K36 were genetically fused via homologous recombination at the gene level, and the resulting construct was then transfected into competent Escherichia coli DH5α cells (Novagen, The U.S.A). Plasmids encoding Gpnmb-K36 were acquired following the amplification and cultivation of the competent cells. Ultimately, the pET25b-Gpnmb and pET25b-Gpnmb-K36 expression vectors were introduced into chemically competent E. coli BLR (DE3) cells (Novagen, The U.S.A). The protocols for protein production were consistent with those previously outlined.[24] For protein purification, please refer to previously published articles from our research group.[25,26] Finally, the high-purity Gpnmb-K36 protein (Figure S1a) was obtained. The Gpnmb-K36 protein was then dissolved in triple-distilled water and its concentration was adjusted to 200 μg/mL in a 1.5 ml centrifuge tube. The solution was placed in a shaker at 4°C, 800 rpm, and shaken for 12 hours. The self-assembled nanovaccine was subsequently obtained and used for further experiments. Similarly, an equimolar concentration of Gpnmb peptide was dissolved in triple-distilled water and subjected to the same procedure.

Characterization of GK-NaV

For transmission electron microscope (TEM) analysis, the samples were readied on copper specimen grids which were covered by a carbon support film. These grids were positioned with the carbon film facing downwards and placed right on top of a 10 μl droplet containing nanoparticles suspension (at a concentration of 10 μg/ml in H_2O). Subsequently, the grids were left to dry at 37°C for 6 hours. Finally, images were observed through a 200 kV TEM (JEOL-2010, Japan). Similarly, the samples were subjected to energy dispersive spectrometer analysis after being prepared on silicon wafers.

In the case of dynamic light scattering (DLS) and Zeta potential analysis, the samples were first completely lyophilized. After that, they were redissolved in H_2O within a 1.5 ml tube to achieve a concentration of 1 mg/ml. Then, the DLS and Zeta potential of the prepared samples were examined using a Zetasizer Nano ZS (Malvern Instruments, UK).

Acquisition of bone marrow-derived dendritic cells (BMDCs)

Female wild-type C57BL/6 mice aged 6–8 weeks were used to obtain bone marrow-derived dendritic cells (BMDCs) under aseptic conditions. The femurs and tibias of these mice were the sources for extracting BMDCs. Subsequently, the BMDCs were seeded in 6-well culture plates, with 2 ml of RPMI 1640 complete medium (at a density of 1×10^6 cells/ml) added to each well. This complete medium contained 10% fetal bovine serum (Inner Mongolia Opcel Biotechnology Co., Ltd), along with interleukin-4 (IL-4) at a concentration of 10 ng/ml (PeproTech, The U.S.A) and granulocyte-macrophage colony-stimulating factor (GM-CSF) at a concentration of 20 ng/ml (PeproTech, The U.S.A). Then, the seeded BMDCs were placed in a cell incubator for culturing. On the 2nd and 4th days of culturing, the original culture medium was replaced with fresh culture medium that had been supplemented with IL-4 (10 ng/ml) and GM-CSF (20 ng/ml). Finally, on the 6th day, the immature BMDCs were collected to be used in further experiments.

Animals immune model

All animal experiments adhere to the ARRIVE guidelines and are carried out in line with the U.K. Animals (Scientific Procedures) Act of 1986, as well as the related guidelines and

EU Directive 2010/63/EU regarding animal experiments. The C57BL/6 mice were procured from Changsheng Company (Shenyang, China). In this study, an HFD was employed to accelerate aging in mice and to induce the emergence of age-related pathological phenotypes.[7,15] These mice were provided with an HFD starting from the age of 4 weeks. At 8 weeks of age, the mice were administered 100 µl of the vaccines via subcutaneous injections (200 µg/ml Gpnmb or GK-NaV). Immunological analysis was carried out when they reached 9 weeks of age, and then efficacy analysis was performed at 48 weeks of age.

Phagocytosis of antigens, intracellular distribution, and surface presentation in dendritic cells

BMDCs were placed in an incubation environment with either Gpnmb-FITC-loaded Gpnmb or GK-NaV (keeping the Gpnmb concentration at 5 µg/ml) for 4 hours. Subsequently, the cells were rinsed using PBS. Next, they were stained with 4′,6-diamidino-2-phenylindole (DAPI) (Beyotime, China) for 5 minutes. Finally, the phagocytosis of Gpnmb was observed through a confocal laser scanning microscope.

For the intracellular distribution analysis, BMDCs were incubated with Gpnmb-FITC-loaded Gpnmb or GK-NaV for 24 hours. Following incubation, the cells were washed with PBS and stained with Lysotracker Deep Red and Hoechst 33,342 for nuclear visualization (Beyotime, China) for 25 minutes. Fresh medium was then added, and the intracellular localization of Gpnmb was examined using a confocal laser scanning microscope.

In the surface presentation studies, after being treated for 36 hours, the BMDCs were incubated with FITC-conjugated H-2K^b/Gpnmb (RRGDGRWKD) tetramer (GENEWIZ, The U.S.A) for 60 minutes. Subsequently, the cells were washed with PBS. Then, they were stained with DAPI (Beyotime, China) for 5 minutes. Finally, the surface presentation of Gpnmb was observed under a confocal laser scanning microscope.

Acquisition of spleen lymphocytes and sorting of CD8$^+$ T cells

Once the mice were euthanized, their spleens were taken out and then dispersed to form single-cell suspensions in mouse lymphocyte isolate (DAKEWEI, China). Subsequently, the cells were passed through a strainer (Thermo Fisher Scientific, The U.S.A) twice in order to get rid of any remaining tissue fragments. After that, the cells were centrifuged at 3000 rpm for 10 minutes and then resuspended in ACK lysis buffer (Biosharp, China) for the purpose of removing erythrocytes. After being incubated for 5 minutes, the cells were washed with PBS three times. Eventually, the lymphocytes were centrifuged again and then resuspended in RPMI 1640 complete medium.

The spleen lymphocytes were resuspended in a sorting buffer. Then, 100 µl of the cell suspension (containing 1×10^7 cells) was added to the flow cytometry tubes. After that, 2 µl of Biotin Antibody Mix (Beaver, China) was added to the tubes. The resulting mixture was incubated at 4°C for 10 minutes. Next, 20 µl of BeaverBeads (Beaver, China) along with Streptavidin (Beaver, China) were put into the flow cytometry tubes. The contents were thoroughly mixed and then incubated at 4°C for another 10 minutes. Subsequently, 2.5 ml of the sorting buffer was added into the flow cytometer tubes. The sorting flow tube containing the cells was then placed on a magnetic rack for 5 minutes. After that, the cell suspension was carefully transferred into a sterile centrifuge tube which housed the purified mouse CD8$^+$T cells. Finally, after centrifugation, the CD8$^+$T cells were obtained.

Isolation of adipocytes and cardiomyocytes

After euthanizing the mice, the visceral adipose and cardiac tissue were collected and minced as finely as they could be. Subsequently, the tissue was put into a composite enzyme digestion solution (with the concentrations of different enzymes being as follows: Collagenase I at 1 mg/ml, Collagenase II at 0.5 mg/ml, Collagenase IV at 0.5 mg/ml, and Trypsin at 0.25 mg/ml) in a ratio of 1:10 and then incubated at 37°C for 40 minutes. After the digestion process was completed, the reaction was stopped by adding DMEM supplemented with 10% FBS. Then, the mixture was centrifuged at 400 g for 5 minutes. Finally, the pellet obtained was resuspended in PBS for the subsequent flow cytometry analysis.

Flow cytometry

The single-cell suspensions from various treatment groups were washed with PBS three times. Subsequently, the cells were stained with fluorescence-labeled antibodies at 4°C for 30 minutes. After that, the cells were centrifuged and then washed with PBS twice before being analyzed by flow cytometry. The flow cytometry panel consisted of the following antibodies (BioLegend, The U.S.A): APC-CD11c, FITC-CD80, PE-CD86, FITC-CD8, PE-CD69, APC-CD25, PE-IFNγ, APC-GzmB, PE-PDL1, PE-CD44, APC-CD62L, and PE-CD31. The antibody of eFluor™ 660-Gpnmb (Thermo Fisher Scientific, The U.S.A) was excited by APC. The data were collected on a BD FACS CantoII flow cytometer.

Histological analyses

Tissue samples were gathered and then fixed overnight in 10% formalin. After that, they were processed and embedded in paraffin. The paraffin sections underwent hematoxylin and eosin (HE) staining following standard procedures. For HE staining of adipose tissue, the cross-sectional areas of adipocytes were measured with the help of an Image analyzer (Keyence). Additionally, for WGA staining, following heat-induced antigen repair using the EDTA antigen repair buffer, the slides of cardiac tissue were incubated with FITC-conjugated WGA (Sigma-Aldrich, located in St. Louis, MO, USA) for 1 hour at 37°C. After that, the slides were stained with DAPI for 10 minutes. Images of the stained sections were taken by observing them under an inverted light microscope or a fluorescence microscope (IX73, Olympus, Japan). Six

different fields in each section were randomly selected for analysis with the help of ImageJ software (The US National Institutes of Health, located in Bethesda, MD, USA).

Senescence-associated (sa)-β-galactosidase (gal) assay

The visceral adipose tissue (The white adipose tissue connected to the epididymis) was collected from mice that had been induced by an HFD. It was then sliced into pieces that were around 1 mm thick and fixed at room temperature for 30 minutes. Subsequently, the tissue slices were incubated overnight at 37°C with the freshly prepared SA-β-gal staining solution (Beyotime, Shanghai), following the manufacturer's instructions. Eventually, the stained adipose tissue was photographed and analyzed using ImageJ software.

Immunoblot analysis

The adipose or cardiac tissues of mice were homogenized in lysis buffer to obtain tissue lysates. Subsequently, the lysates (40–50-μg) were resolved by SDS – polyacrylamide gel electrophoresis. After that, the proteins were transferred onto PVDF membranes (Millipore, The U.S.A). These membranes were then incubated with the primary antibody, and afterward, they were incubated with horseradish peroxidase-conjugated antirabbit or antimouse immunoglobulin-G (Jackson, The U.S.A). Enhanced chemiluminescence (Amersham, Sweden) was used to detect specific proteins. The primary antibodies (Proteintech, The U.S.A) for immunoblotting included Gpnmb, P53, P21, P16 and GAPDH. All of these primary antibodies were diluted at a ratio of 1:1000, with the exception of the GAPDH antibody, which was diluted at 1:2000. The secondary antibody was peroxidase-conjugated AffiniPure goat anti-mouse IgG (light chain specific) (Proteintech, The U.S.A). All secondary antibodies were added at a dilution of 1:2000. The immunoblot images were acquired using the Tanon 4600 (China).

Assessment of systemic metabolic parameters

Before the experiments began, the mice were housed individually for one week. On the day when the glucose tolerance test (GTT) was conducted, the mice were fasted for six hours. Then, in the early afternoon, they received an intraperitoneal injection of glucose at a dosage of 1 g/kg of their body weight. Regarding the insulin tolerance test (ITT), human insulin was administered intraperitoneally to the mice at a dose of 1 U/kg of their body weight. Blood samples were then collected from the tail vein at 0, 15, 30, 60, and 120 minutes after the administration of each agent. Subsequently, the blood glucose levels were measured by using a glucose analyzer (Sanwa Kagaku Kenkyusho).

Echocardiography

Cardiac function was evaluated by means of transthoracic echocardiography. Briefly, after the chest hair of the mice was shaved, they were anesthetized with pentobarbital. Then, the mice were placed flat on their backs on a plate. Subsequently, parameters such as left ventricular ejection fraction (EF), left ventricular fractional shortening (FS), left ventricular posterior wall thickness in diastole (LVPWd), left ventricular internal diameter in diastole (LVIDd), and the mitral valve (MV) E/A ratio were measured through echocardiography.

Statistical analysis

The data are represented as mean ± standard deviation (SD), and each experiment was performed at least three times, with more than three replicates for each trial. Representative data from four independent experiments with similar results. Survival curves were drawn by the Kaplan – Meier method and compared with the log-rank test. GraphPad Prism 8.0 and FlowJo v10 software were used for constructing graphs and analyzing flow cytometry data, respectively. Groups were compared by one-way analysis of variance using GraphPad Prism software package: $^{****}p < .0001$, $^{***}p < .001$, $^{**}p < .01$, and $^{*}p < .05$.

Results

Synthesis and characterization of GK-NaV

GK-NaV is created by fusing seno-antigen peptides Gpnmb with the cationic protein K36. Gpnmb seno-antigens are endogenous type 1 transmembrane glycoproteins that are specifically expressed in senescent cells.[7,27] The Gpnmb peptides, derived from seno-antigens, were cloned and engineered alongside K36, which features a highly repetitive unit characterized by $(VPGKG)_{36}$. This process resulted in the formation of the cationic fusion protein Gpnmb-K36 (GK36) (Figure 1a). Through hydrogen bonding interactions formed between amino acid residues, this fusion protein self-assembles to form structurally stable, spherical-like nanovaccine GK-NaV (Figure 1b), and the mean sizes of GK-NaV detected by dynamic light scattering (DLS) were about 15 nm in an aqueous solution (Figure 1c), as well as the zeta potentials of GK-NaV were about +9.6 mV (Figure 1d). Remarkably, the energy dispersive spectrometer reveals that the primary elements constituting GK36 include carbon (C), oxygen (O), nitrogen (N), phosphorus (P), and sulfur (S), which aligns with the compositional constituents of proteins (Figure 1e). Furthermore, to investigate the stability of GK-NaV under neutral conditions, GK-NaV was incubated in PBS at pH 7.5 at 37°C. At various time points, the degradation of GK-NaV was observed by SDS-PAGE and the concentration of Gpnmb was detected by ELISA. The results indicated that GK-NaV remained intact for over 8 days (Figure S1a), with the concentration of Gpnmb gradually increased after 8 days (Figure 1f). To evaluate the biocompatibility of GK-NaV, BMDCs were cultured with PBS, Gpnmb, and GK-NaV at concentrations of 25, 50, 100, 200 μg/ml. Cytotoxicity assays showed that the treatments did not significantly affect cell viability (Figure S1b).

GK-NaV effectively promoted robust cross-presentation to $CD8^+$ T cells

To verify the activation effect of GK-NaV on antigen-presenting cells, we co-cultured BMDCs with PBS, Gpnmb,

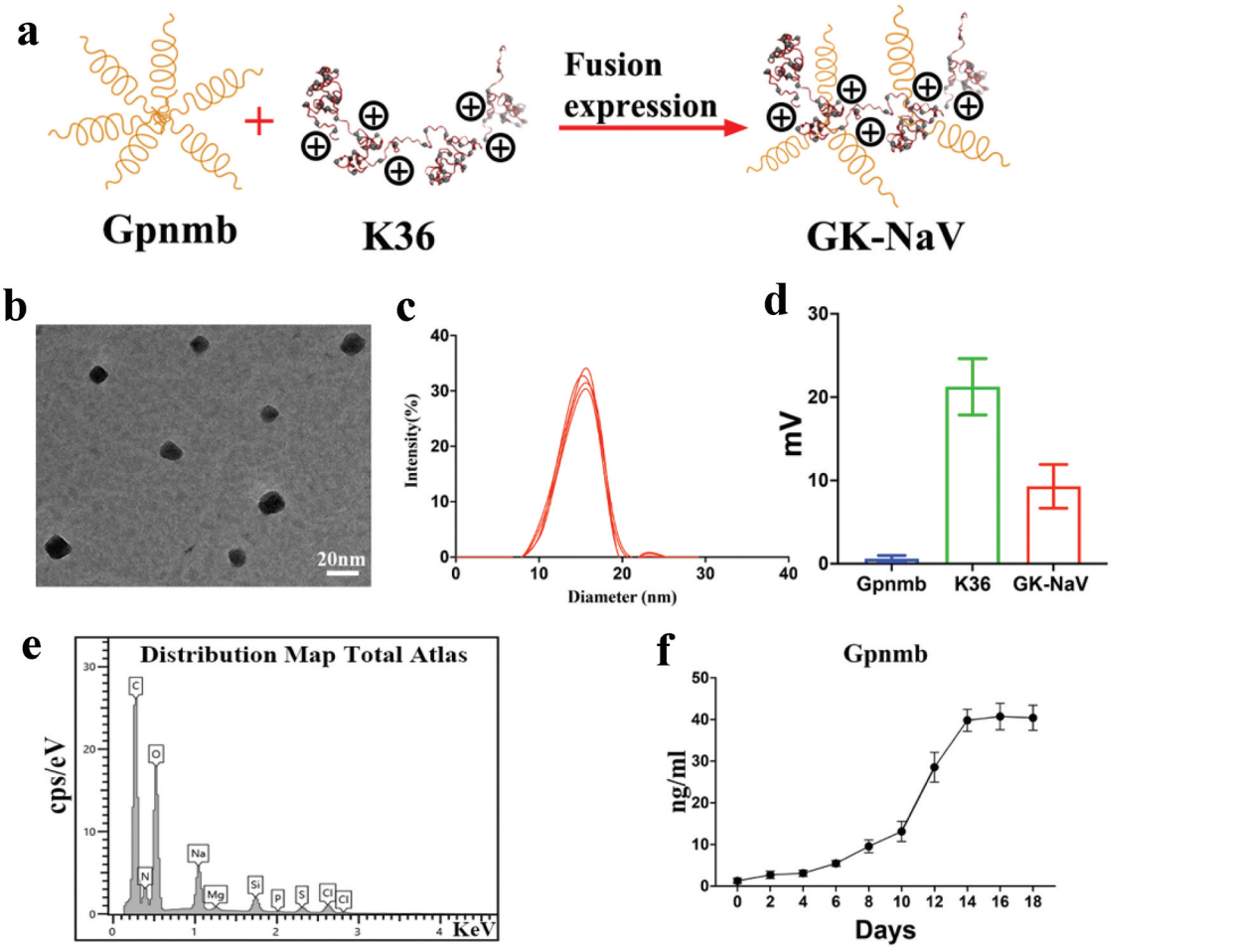

Figure 1. Synthesis and characterization of GK-NaV. (a) The synthesis routes of the GK-NaV. (b) Representative transmission electron microscope (TEM) image of the GK-NaV ($n = 4$). (c) The particle size and distribution of GK-NaV were measured by dynamic light scattering (DLS) ($n = 4$). (d) Zeta potential of Gpnmb, K36 and GK-NaV ($n = 4$). (e) Energy dispersive spectroscopy was utilized to analyze the primary elemental composition of GK-NaV. (f) The concentration of Gpnmb was determined using ELISA ($n = 4$).

and GK-NaV in vitro. After a 4-hour co-culture, BMDCs in the GK-NaV group showed significantly enhanced uptake of Gpnmb antigen (Gpnmb-FITC) compared to the other groups, while a moderate level of phagocytosis of Gpnmb-FITC was noted in the Gpnmb group as well (Figure S2a). Following 24 hours of co-culture, we performed a cellular distribution experiment. As shown in Figure 2, GK-NaV resulted in a notable increase in cytosolic peptide fluorescence, which is quantified in Figure S2b according to the method described in reference.[28] In contrast, in the groups pre-treated with Gpnmb, the majority of the Gpnmb-FITC was found within lysosomes, with only a faint fluorescence signal detected in the cytoplasm. This suggests that GK-NaV has strong transmembrane capabilities and exhibits remarkable lysosomal escape activity. We subsequently found that after 36 hours, GK-NaV resulted in a significantly greater surface presentation of Gpnmb compared to free Gpnmb. This was demonstrated by the staining of Gpnmb–H-2K^b complexes on the surface of BMDCs using a specific antibody (Figure 2b). This finding highlights the unique advantage of GK-NaV in facilitating antigen cross-presentation. Notably, the maturation of DCs is essential for effective antigen presentation and the initiation of subsequent immune responses.[29,30] We then evaluated the maturation of BMDCs using flow cytometry after 48 hours of treatment with different formulations. Remarkably, BMDCs that were pulsed with GK-NaV showed the most significant upregulation of co-stimulatory molecules (CD80 and CD86) when compared to those treated with free Gpnmb or PBS (Figure 2c,d, S2c, S2d). In line with the maturation data of BMDCs, those treated with GK-NaV demonstrated the greatest production of IL-12 (Figure 2e). Additionally, BMDCs were incubated with PBS, Gpnmb, and GK-NaV for 48 hours. The treated BMDCs were subsequently co-incubated with sorted Carboxyfluorescein succinimidyl ester (CFSE)-labeled mouse CD8$^+$ T cells for an additional 36 hours. Flow cytometry results indicated that BMDCs treated with GK-NaV were more effective in stimulating the proliferation of CD8$^+$ T cells compared to those treated with free Gpnmb or PBS (Figure 2f,g). These findings demonstrate that GK-NaV enhances the intracellular delivery of antigens, induces sustained antigen presentation, and leads to the maturation of DCs. Consequently, this process promotes the effective cross-priming of CD8$^+$ T cells.

GK-NaV immunization induced specific cellular immunity

Motivated by the encouraging in vitro results, we aimed to evaluate the immunization efficacy of GK-NaV in vivo.

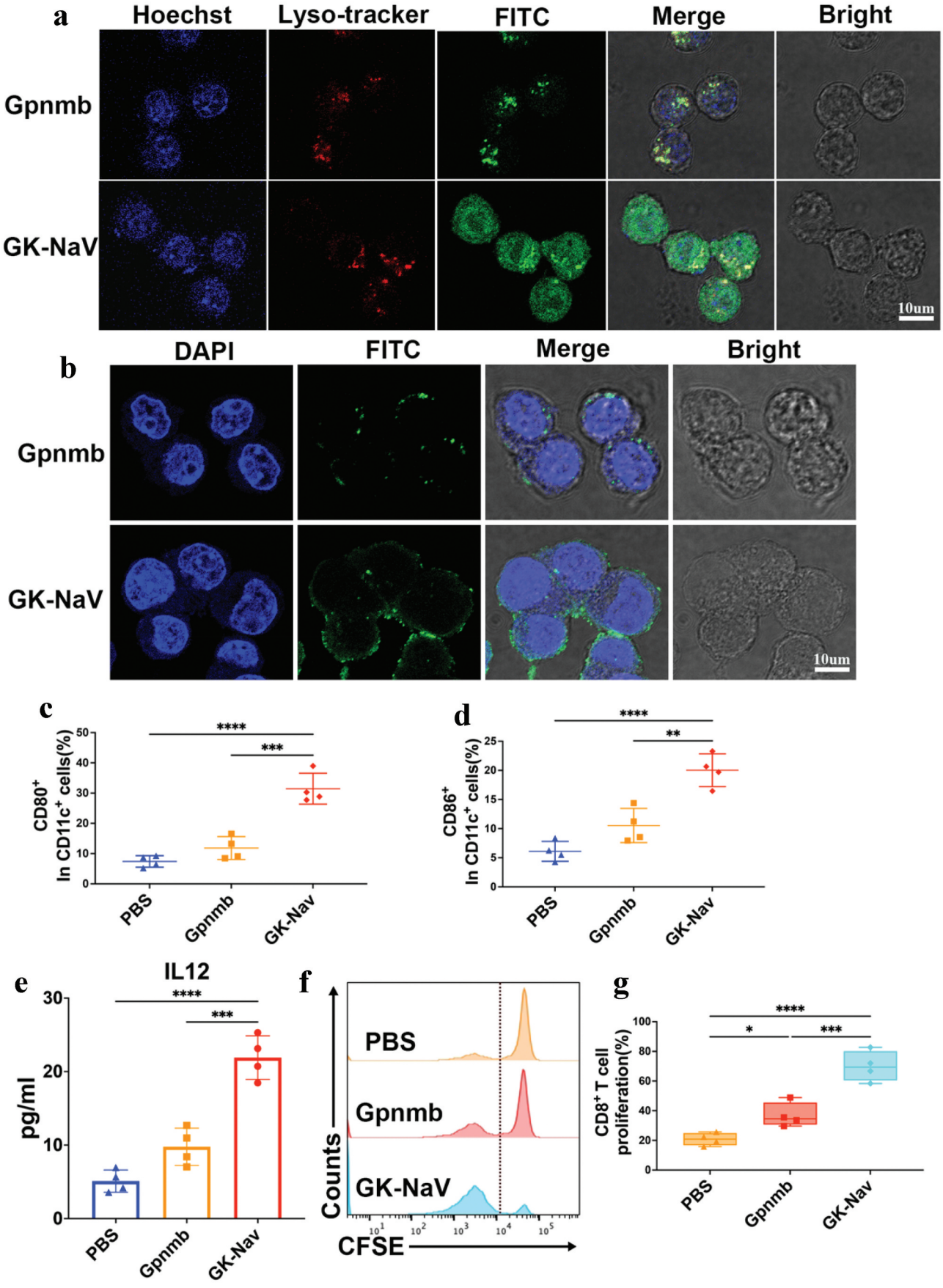

Figure 2. GK-NaV induced strong cross-presentation to $CD8^+$ T cells. (a) The cytosolic delivery of Gpnmb in BMDCs was observed using confocal laser scanning microscopy (CLSM) ($n = 4$). Blue, nucleus; red, lysosomes stained with Lyso-Tracker Deep red; green, Gpnmb-FITC. (b) Staining of the H-$2K^b$-Gpnmb complex to assess surface presentation of Gpnmb by BMDCs after incubation with Gpnmb and GK-NaV for 36 hours. Blue, nucleus; green, antibody against H-K^b-Gpnmb ($n = 4$). (c, d) Quantitative analysis of CD80 and CD86 expression on $CD11c^+$ BMDCs ($n = 4$). (e) The secretion of IL12 by BMDCs following treatment with PBS, Gpnmb and GK-NaV was detected by ELISA ($n = 4$). (f) The proliferation of $CD8^+$ T cells was assessed by flow cytometry ($n = 4$). (g) Quantitative data on proliferation of $CD8^+$ T cells.

C57BL/6 mice were placed on an HFD starting at 4 weeks of age. They received subcutaneous vaccinations at 8 weeks of age, and subsequent immunological analyses were conducted at 9 weeks (Figure 3a). Firstly, we employed intravital imaging to examine the retention kinetics of Gpnmb and GK-NaV at the injection site following subcutaneous administration (Gpnmb labeled with Cy5). As shown in Figure 3b, GK-NaV group exhibited a notable antigen retention effect, displaying gradual clearance with distinct fluorescence still visible at 7 days. In contrast, the fluorescence signals in the Gpnmb group diminished rapidly, nearly disappearing by 1 day after injection (Figure 3b, Figure S3a). Furthermore, Consistent with the in vitro experiments, GK-NaV significantly enhanced the maturation of DCs (upregulation of CD80 and CD86) in the inguinal lymph nodes of mice compared to the control group (Figure 3c,d, S3B, S3C). As anticipated, we observed that GK-NaV vaccination significantly elevated the expression of CD25 (Figure 3e, S3d) and CD69 (Figure 3f, S3e) on $CD8^+$ T cells in mouse lymph nodes, indicative of $CD8^+$ T cell activation, when compared to the PBS and Gpnmb groups. Likewise, GK-NaV vaccination increased the proportion of $CD8^+$ IFN-γ^+ (Figure 3g, S3f) and $CD8^+$ $GzmB^+$ (Figure 3h, S3g) T cells in the lymph nodes. In addition, the safety profiles of GK-NaV formulations in vivo were evaluated through histopathological analysis to assess any abnormalities in the major organs. Our observations revealed no pathological lesions in any of the treated groups (Figure S3H). These findings suggested that GK-NaV vaccination markedly enhanced specific cellular immunity in a mouse model induced by an HFD.

GK-NaV vaccination alleviated metabolic disorders in adipose tissue in progeroid mice induced by an HFD

We then assessed the potential of GK-NaV vaccination to alleviate metabolic disorders in mice fed an HFD. C57BL/6

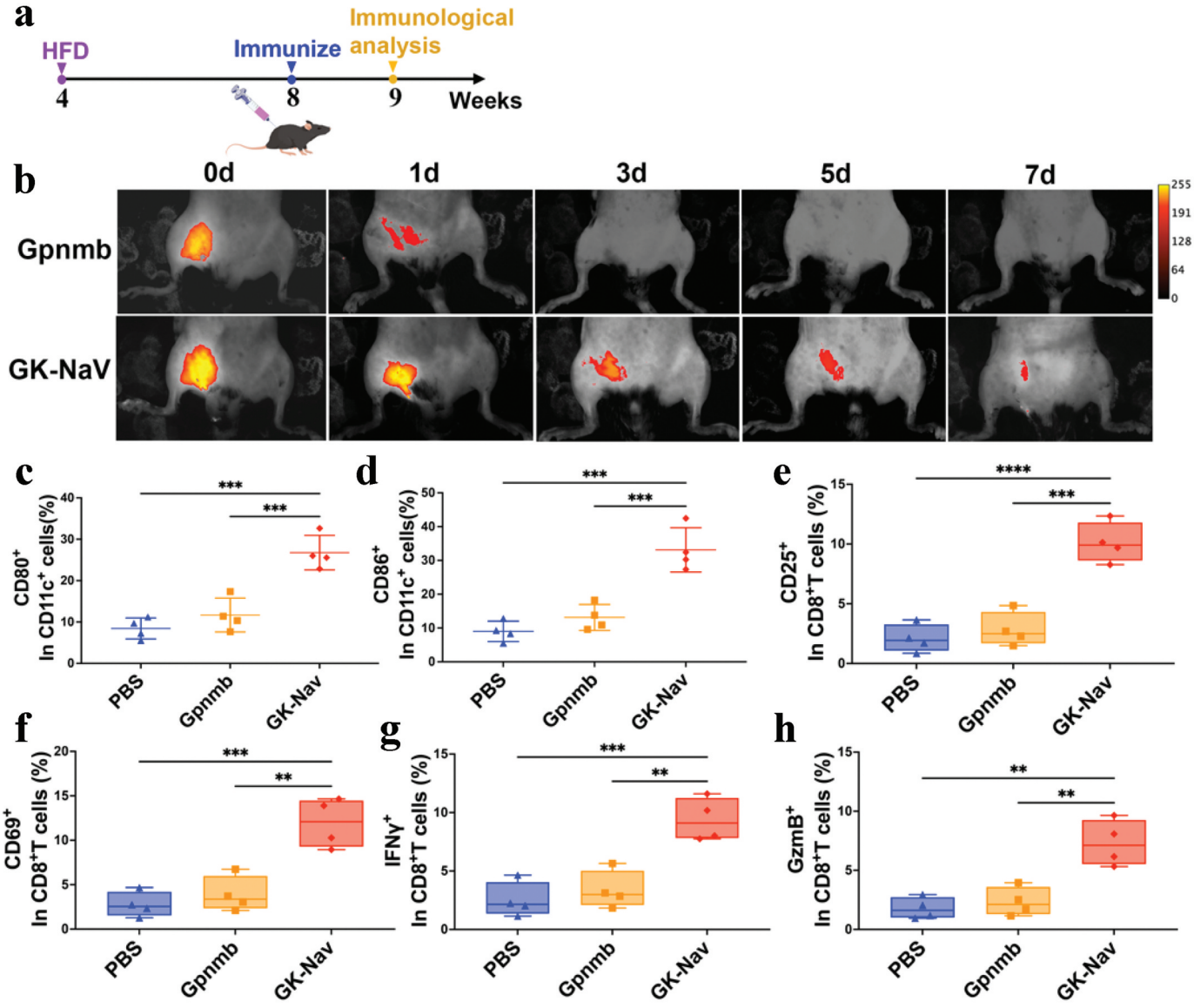

Figure 3. GK-NaV immunization induced specific cellular immunity. (a) Timeline of vaccination and immunological analysis in C57BL/6 mice. (b) Representative fluorescence images of mice subcutaneously injected with Gpnmb and GK-NaV ($n = 4$). (c, d) Quantitative flow cytometric analysis of $CD80^+$ and $CD86^+$ BMDCs gating on $CD11c^+$ cells in lymph nodes (LNs) of different groups ($n = 4$). Quantitative flow cytometric analysis of $CD8^+CD25^+$ (e) and $CD8^+CD69^+$ (f) T lymphocytes in LNs of mice ($n = 4$). Quantitative flow cytometric analysis of $CD8^+IFN\gamma^+$ (G) and $CD8^+GzmB^+$ (H) T lymphocytes in LNs of mice ($n = 4$).

mice were fed an HFD starting at 4 weeks of age. They received subcutaneous vaccinations at 8 weeks of age, and the effects were analyzed at 48 weeks (Figure 4a, S4a). We found that the administration of GK-NaV significantly decreased senescence-associated β-galactosidase (SA-β-gal) activity in visceral adipose tissue compared to the PBS and Gpnmb groups (Figure 4b). Additionally, it downregulated the expression of senescence markers P16, P21, and P53, as confirmed by the immunoblot analysis (Figure 4c, S4b). Likewise, immunization with GK-NaV significantly reduced Gpnmb expression in visceral adipose tissue, as confirmed by immunoblot (Figure 4c, S4b). Flow cytometry similarly confirmed a notable reduction in Gpnmb expression in adipocytes rather than in epithelial cells within adipose tissue (downregulation of $CD31^{-}Gpnmb^{+}$) (Figure 4d, S4c). This finding underscores the effectiveness of the vaccine in specifically targeting and eliminating Gpnmb-positive senescent cells. Furthermore, histological analysis of visceral adipose tissue demonstrated a marked decrease in the average cross-sectional area of adipocytes in the GK-NaV group compared to the PBS and Gpnmb groups (Figure 4e,f).[31,32] Importantly, in the glucose tolerance test (GTT) and insulin tolerance test (ITT) assays, we observed that the administration of GK-NaV prominently enhanced metabolic profiles, including improvements in glucose tolerance (Figure 4g) and insulin resistance (Figure 4h), both of which are major metabolic disorders associated with adipocyte senescence.[7,32] In addition, to investigate the effects of the GK-NaV vaccination on lifespan, we assessed the survival rate of the mice. Our findings revealed that administration of the GK-NaV noticeably extended the median lifespan of the mice (the median survival times for the PBS, Gpnmb, and GK-NaV groups were 86.5 ± 1.85 weeks, 89 ± 1.6 weeks, and 101 ± 1.45 weeks, respectively) (Figure 4i). Further, the immune memory activity was analyzed in the 48th week of the HFD feeding. We quantified the proportions of $CD44^{+}CD62L^{+}$ central memory T cells (Tcm) and $CD44^{+}CD62L^{-}$ effector memory T cells (Tem) within the $CD8^{+}$ T cell population in the mouse lymph nodes using flow cytometry. Our results indicated that, compared to the PBS and Gpnmb groups, the GK-NaV treatment elicited the highest proportions of both Tcm and Tem (Figure 4j, S4d). These results confirm that GK-NaV immunization effectively targets the elimination of Gpnmb-positive senescent adipocytes, leading to a significant improvement in the metabolic disorders induced by the HFD. In addition, to further validate the long-lasting anti-aging immune effects triggered by the GK-NaV, we assessed lymph node immune memory activity and the expression level of SA-β-gal in the visceral adipose tissue of mice at the 50th and 52nd weeks of HFD feeding. We found that, compared to the PBS and Gpnmb groups, the GK-NaV immunized group still induced the highest levels of Tcm and Tem in the lymph nodes of mice (Figure S4e). Likewise, SA-β-gal activity in visceral adipose tissue was significantly lower in the GK-NaV group compared to the PBS and Gpnmb groups (Figure S4f).

GK-NaV vaccination improved cardiac dysfunction in progeroid mice induced by an HFD

Next, to further validate the targeted clearance effect of the GK-NaV on senescent cells, we explored the impact of the GK-NaV on aging-related cardiac dysfunction in the HFD-induced progeroid mice model. Similar to the findings in adipose tissue, immunoblot analysis revealed that the expression of senescence markers P16, P21, and P53 in the cardiac tissue of the GK-NaV group was remarkably lower than that in the PBS and Gpnmb group (Figure 5a, Figure S5a). Similarly, immunization with GK-NaV resulted in a notable reduction in Gpnmb expression in cardiac tissue, as verified by immunoblot analysis (Figure 5a, Figure S5a). Flow cytometry also demonstrated a marked decrease in Gpnmb expression specifically in cardiomyocytes, rather than in the epithelial cells of the cardiac tissue (evidenced by the downregulation of $CD31^{-}Gpnmb^{+}$) (Figure 5b, Figure S5b). Importantly, in echocardiographic assessments of the mice, we observed that the GK-NaV substantially improved cardiac dysfunction compared to the PBS and Gpnmb groups, evidenced by an increase in left ventricular ejection fraction (EF) and left ventricular fractional shortening (FS), a reduction in left ventricular posterior wall diastolic thickness (LVPWd) and the diastolic left ventricular internal diameter (LVIDd), and alleviation of left ventricular diastolic dysfunction (MV E/A) (Figure 5c). Furthermore, histological analysis of cardiac tissue revealed a significant reduction in the average cross-sectional area of cardiomyocytes in the GK-NaV group compared to the PBS and Gpnmb group mice (Figure 5d). Additionally, to assess the biotoxicity of GK-NaV, the body weight of the mice was closely monitored. Our observations revealed no significant differences in body weight changes among the different groups (Figure S5c). These findings indicate that the GK-NaV can selectively target and eliminate $Gpnmb^{+}$ senescent cells in cardiac tissue, resulting in a marked improvement of cardiac function in progeroid mice induced by an HFD.

Discussion

The accumulation of senescent cells within tissues can lead to aging-related functional disruptions in the organism.[32–34] Growing evidence has shown that the targeting and removal of senescent cells using anti-aging vaccines can mitigate metabolic abnormalities associated with aging.[7,15,27] For instance, a vaccine designed to target CD153-expressing senescent T cells significantly enhanced glucose metabolism in obese mice.[15] Intriguingly, recent efforts aimed at selectively targeting senescent cells linked to various pathologies have led to the development of a peptide vaccine that specifically targets endothelial cells exhibiting elevated levels of Gpnmb, which has recently been identified as a biomarker of senescence.[7,31,35–37] However, peptide-based

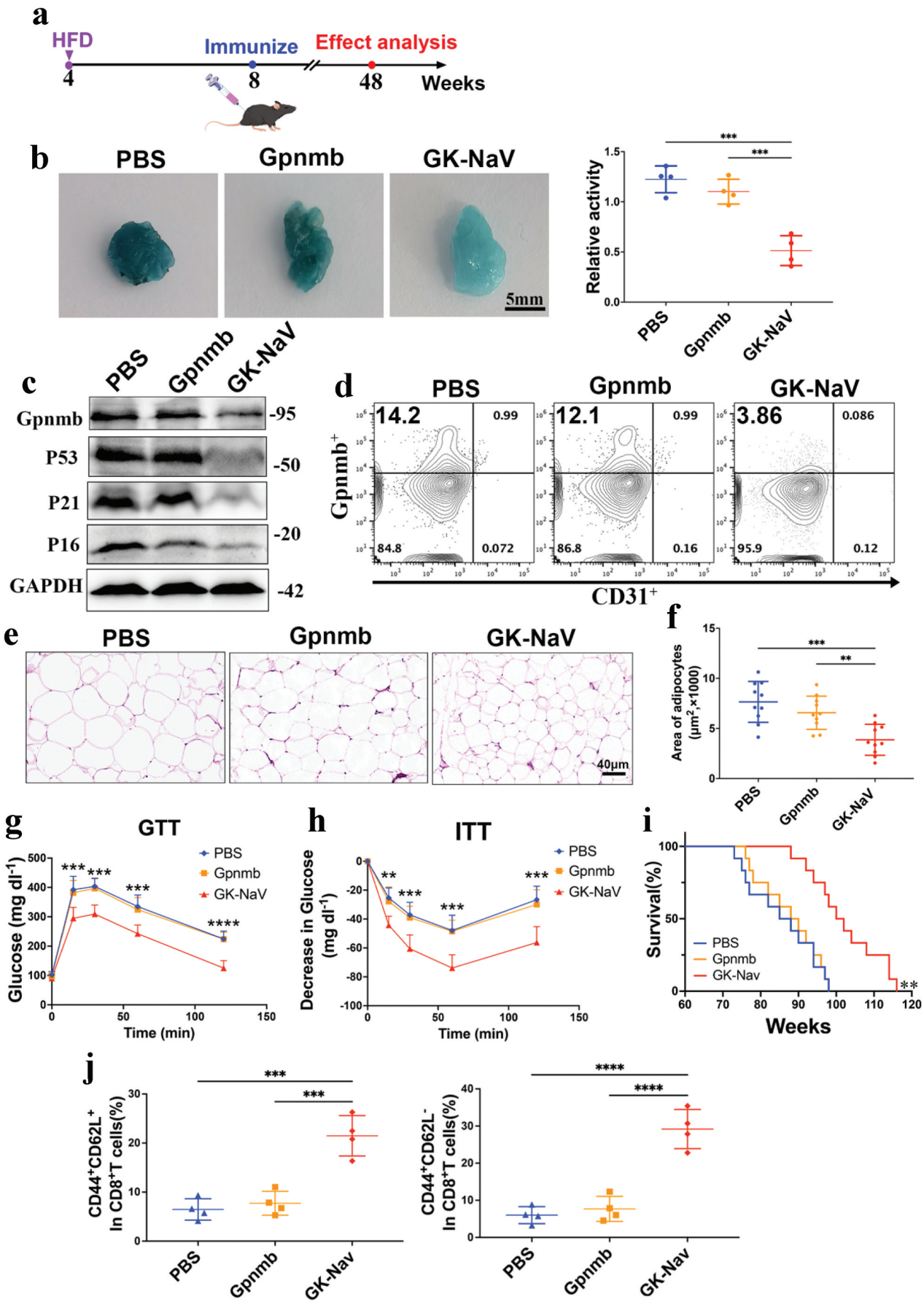

Figure 4. GK-NaV vaccination alleviated metabolic disorders in adipose tissue in progeroid mice induced by an HFD. (a) Timeline of vaccination and effect analysis in C57BL/6 mice. (b) SA-β-gal assay of visceral adipose tissue obtained from PBS, Gpnmb and GK-NaV groups of mice and the quantification of sa-β-gal activity ($n = 4$). (c) Immunoblot analysis was conducted to assess the activation levels of Gpnmb, P16, P21, and P53 in adipose tissue, utilizing specific antibodies for each target protein

vaccines often suffer from poor stability, weak immunogenicity, and typically induce only short-term immune responses.[38–40] Importantly, aging is a chronic process characterized by the continuous production and accumulation of senescent cells, which can lead to metabolic dysfunction within tissues.[3,41,42] Therefore, an anti-aging vaccine need not only generate a specific immune response targeting the senescence-specific antigens but also effectively induce long-lasting immune memory and efficiently activate the immune cells of the aging organism.

Based on the unique characteristics of aging, we have created a novel anti-aging nanovaccine (GK-NaV) by fusing cationic

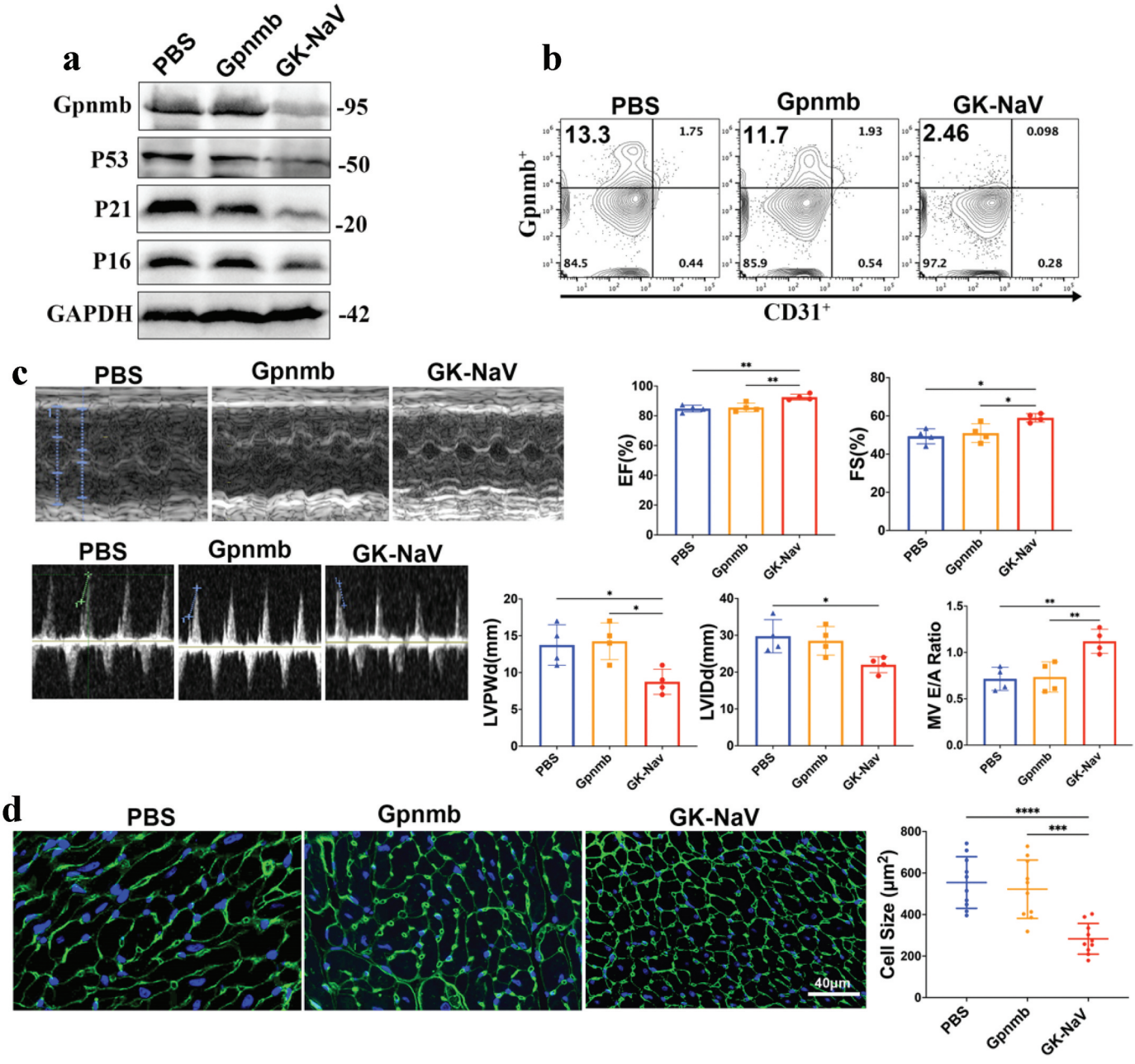

Figure 5. GK-NaV vaccination improved cardiac dysfunction in progeroid mice induced by an HFD. (a) Immunoblot analysis was conducted to assess the activation levels of Gpnmb, P16, P21, and P53 in cardiac tissue, utilizing specific antibodies for each target protein, GAPDH was used as an internal reference. (b) Cardiac tissue was digested into single cells, $CD31^{-}Gpnmb^{+}$ cardiomyocytes were analyzed by flow cytometry ($n = 4$). (c) Representative echocardiography and cardiac parameters measured via echocardiography ($n = 4$). (d) WGA staining of the cardiac tissue for assessing cardiomyocyte size in cross-sections of the heart and the statistical data ($n = 10$).

($n = 3$), GAPDH was used as an internal reference. (d) Adipose tissue was digested into single cells, $CD31^{-}Gpnmb^{+}$ adipocytes were analyzed by flow cytometry ($n = 4$). (e) Representative pictures of hematoxylin and eosin (HE) staining of visceral adipose tissue ($n = 10$). (f) Quantification of adipocyte cross-sectional area (>150 adipocytes per animal) ($n = 10$). Glucose tolerance test (GTT) (G) and insulin tolerance test (ITT) (H) in PBS, Gpnmb and GK-NaV groups of mice (at 48 weeks old) ($n = 10$), the changes from basal glucose levels are shown in the ITT graph. (i) The survival time of mice in PBS, Gpnmb and GK-NaV groups ($n = 12$). (j) Quantitative flow cytometric analysis of $CD44^{+}CD62L^{+}$ central memory T cells (Tcm) and $CD44^{+}CD62L^{-}$ effector memory T cells (Tem) in lymph nodes of mice ($n = 4$).

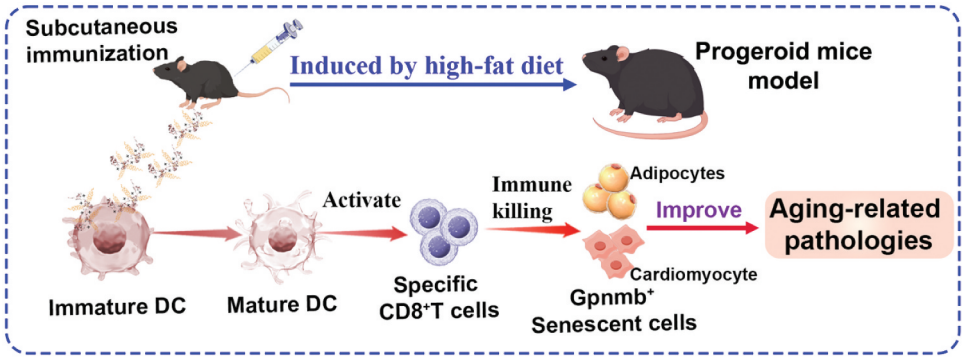

Figure 6. Nanovaccines loaded with seno-antigen elicit specific anti-aging immune responses through subcutaneous immunization, targeting and eliminating senescent cells to improve aging-related pathologies.

protein (K36) with the seno-antigen peptide Gpnmb (Figure 1a). The high stability of GK-NaV endows them with a significant antigen reservoir effect (Figures 1f, 3b), which is a crucial prerequisite for the activation of immune responses.[17,39] Further, the surface charge of nanovaccines plays a critical role in facilitating the delivery of antigens to dendritic cells (DCs) and in stimulating immune responses. In contrast to anionic nanovaccines, cationic nanovaccines have been shown to possess superior immunostimulatory properties, including enhanced internalization by DCs, increased T cell proliferation, and improved transport efficiency of antigens.[43,44] In this work, cationic GK-NaV was found to be extensively internalized by DCs (Figure S2A), facilitating their escape from lysosomes (Figure 2a) and promoting cross-presentation of antigens (Figure 2b). Leveraging these advantageous properties of GK-NaV notably enhances the maturation of DCs (Figures 2c,d, 3c,d), thereby increasing the specific cytotoxic activity of $CD8^+$ T cells (Figure 2f,g, 3e–h). Undoubtedly, the induction of immune memory is one of the most important characteristics of vaccination, as it is crucial for ensuring the long-term maintenance of immune surveillance in the body.[45,46] As expected, GK-NaV greatly increased the proportion of central and effector memory $CD8^+$ T cells 40 weeks following subcutaneous immunization (Figure 4j, S4e). Thus, the GK-NaV-activated specific anti-aging immune response selectively targets and eliminates senescent cells within adipose and cardiac tissue (Figure 4b–d, 5a,b). Given that targeting the elimination of senescent cells in vivo has been reported to alleviate various aging and aging-related disorders,[7,41,47,48] we tested whether GK-NaV-mediated elimination of senescence also improves the aging phenotypes. Our research findings demonstrated that GK-NaV immunization remarkably ameliorated the metabolic abnormalities in adipose tissue (Figure 4e–h) and cardiac dysfunction (Figure 5c,d), and also extended the lifespan of the mice (Figure 4i).

This study has some limitations. We acknowledge that aging is the result of multiple factors, such as obesity, oxidative stress, genetic mutations, and the regulation of the senescence-associated secretory phenotype (SASP). The mechanisms underlying aging may vary depending on the different factors involved. However, in this study, we only used a high-fat diet to establish a model for inducing aging in mice, which presents certain limitations. Further, although the experiment demonstrated the vaccine's efficacy, the lack of a multi-dose gradient for GK-NaV is a limitation. Future studies should explore multiple vaccine dosage gradients to evaluate the range from suboptimal protection at lower doses to potential adverse reactions or immune overactivation at higher doses. In addition, current anti-aging drugs, such as dasatinib and quercetin, have been shown to clear senescent cells. Although previous study have demonstrated that the anti-aging effects of peptide vaccines are stronger than those of the anti-aging drugs dasatinib and quercetin,[7] it is still necessary to compare the anti-aging effects of the nanovaccine with these drugs in order to fully validate the efficacy of the nanovaccine. This will also serve as a key focus in our future research.

Conclusions

In summary, anti-aging vaccines must be meticulously designed to elicit a potent and sustained anti-aging immune response. Here, we demonstrate that nanovaccines possess substantial advantages in activating specific anti-aging immune cytotoxicity. Consequently, our study opens a new avenue for targeting the elimination of senescent cells and treating age-related pathologies through an anti-aging nanovaccine composed of cationic protein (K36) and seno-antigen peptides (Gpnmb) (Figure 6). These findings indicate that utilizing nanovaccines to target cell- or tissue-specific seno-antigens like Gpnmb could provide a promising strategy for next-generation senolytic therapy with higher selectivity and fewer off-target effects.

Acknowledgments

We extend our gratitude to Professor Jin Haofan for providing the plasmid encoding the K36 and for his valuable suggestions regarding the extraction of proteins from cardiac tissue.

Disclosure statement

No potential conflict of interest was reported by the author(s).

Funding

This work was supported by the Norman Bethune Plan Project of Jilin University under Grant number [2024B32]; Scientific Research Project of the Jilin Provincial Department of Education under Grant [JJKH20241335KJ]; and the Project Agreement for Science & Technology Development, Jilin Province under Grant number [YDZJ202401693ZYTS].

Notes on contributor

Jiyan Leng is a compassionate and highly proficient geriatrician with a profound dedication to enhancing the quality of life for elderly patients. She obtained her medical degree from Jilin university, where she laid a solid foundation in medical knowledge across various disciplines. Subsequently, she pursued specialized training in geriatrics through a fellowship program at the First Hospital of Jilin University, delving deep into the unique medical complexities and challenges that come with aging. Currently, Jiyan Leng is a Chief Physician in the Department of Geriatrics at First Hospital of Jilin University, she specializes in diagnosing and treating various age-related diseases like Alzheimer's disease, hypertension in the elderly, and mobility issues due to osteoarthritis. In the realm of research, Jiyan Leng is committed to investigating the mechanisms underlying the aging of various tissues and organs, as well as the interplay between aging and the immune system. Her research seeks to leverage immunotherapeutic approaches to mitigate the aging process, with the ultimate goal of facilitating "healthy aging" in a true sense for the elderly.

Author contributions

Qiliang Yin and Jiyan Leng provided concepts. Kexin Zhang, Qiliang Yin and Yucen Ma performed the experiments and wrote the manuscript. Mengyu Cao and Lingwei Li collected and analyzed the data. Xinliang Jin and Jiyan Leng revised the manuscript and supervised the experiments.

Data availability statement

The data presented in this study are available from the corresponding author upon request.

Institutional review board statement

All animal experiments comply with the ARRIVE guidelines and are conducted in accordance with the U.K. Animals (Scientific Procedures) Act, 1986, and associated guidelines, EU Directive 2010/63/EU for animal experiments.

Abbreviations

HFD	High-fat diet
BMDCs	Bone marrow-derived dendritic cells
TEM	Transmission electron microscope
DLS	Dynamic light scattering
HE	Hematoxylin and eosin
SA-β-gal	Senescence-associated-β-galactosidase assay
GTT	Glucose tolerance test
ITT	Insulin tolerance test
EF	Ejection fraction
FS	Fractional shortening
LVPWd	Left ventricular posterior wall thickness in diastole
LVIDd	Left ventricular internal diameter in diastole
MV	Mitral valve
CFSE	Carboxyfluorescein succinimidyl ester
CLSM	Confocal laser scanning microscopy

References

1. Kirkland JL, Tchkonia T. Clinical strategies and animal models for developing senolytic agents. Exp Gerontol. 2015;68:19–25. doi:10.1016/j.exger.2014.10.012.
2. Khosla S, Farr JN, Tchkonia T, Kirkland JL. The role of cellular senescence in ageing and endocrine disease. Nat Rev Endocrinol. 2020;16(5):263–275. doi:10.1038/s41574-020-0335-y.
3. Suryadevara V, Hudgins AD, Rajesh A, Pappalardo A, Karpova A, Dey AK, Hertzel A, Agudelo A, Rocha A, Soygur B, et al. SenNet recommendations for detecting senescent cells in different tissues. Nat Rev Mol Cell Biol. 2024;25(12):1001–1023. doi:10.1038/s41580-024-00738-8.
4. Zhao Y, Yue R. Aging adipose tissue, insulin resistance, and type 2 diabetes. Biogerontology. 2024;25(1):53–69. doi:10.1007/s10522-023-10067-6.
5. Baker DJ, Childs BG, Durik M, Wijers ME, Sieben CJ, Zhong J, Saltness RA, Jeganathan KB, Verzosa GC, Pezeshki A, et al. Naturally occurring p16(Ink4a)-positive cells shorten healthy lifespan. Nature. 2016;530(7589):184–189. doi:10.1038/nature16932.
6. Novais EJ, Tran VA, Johnston SN, Darris KR, Roupas AJ, Sessions GA, Shapiro IM, Diekman BO, Risbud MV. Long-term treatment with senolytic drugs dasatinib and quercetin ameliorates age-dependent intervertebral disc degeneration in mice. Nat Commun. 2021;12(1):5213. doi:10.1038/s41467-021-25453-2.
7. Suda M, Shimizu I, Katsuumi G, Yoshida Y, Hayashi Y, Ikegami R, Matsumoto N, Yoshida Y, Mikawa R, Katayama A, et al. Senolytic vaccination improves normal and pathological age-related phenotypes and increases lifespan in progeroid mice. Nat Aging. 2021;1(12):1117–1126. doi:10.1038/s43587-021-00151-2.
8. Palmer AK, Xu M, Zhu Y, Pirtskhalava T, Weivoda MM, Hachfeld CM, Prata LG, van Dijk TH, Verkade E, Casaclang-Verzosa G, et al. Targeting senescent cells alleviates obesity-induced metabolic dysfunction. Aging Cell. 2019;18(3):e12950. doi:10.1111/acel.12950.
9. He S, Sharpless NE. Senescence in health and disease. Cell. 2017;169(6):1000–1011. doi:10.1016/j.cell.2017.05.015.
10. Kirkland JL, Tchkonia T. Cellular senescence: a translational perspective. EBioMedicine. 2017;21:21–28. doi:10.1016/j.ebiom.2017.04.013.
11. Xu M, Pirtskhalava T, Farr JN, Weigand BM, Palmer AK, Weivoda MM, Inman CL, Ogrodnik MB, Hachfeld CM, Fraser DG, et al. Senolytics improve physical function and increase lifespan in old age. Nat Med. 2018;24(8):1246–1256. doi:10.1038/s41591-018-0092-9.
12. Zingoni A, Antonangeli F, Sozzani S, Santoni A, Cippitelli M, Soriani A. The senescence journey in cancer immunoediting. Mol Cancer. 2024;23(1):68. doi:10.1186/s12943-024-01973-5.
13. Onorati A, Havas AP, Lin B, Rajagopal J, Sen P, Adams PD, Dou Z. Upregulation of PD-L1 in senescence and aging. Mol Cell Biol. 2022;42(10):e0017122. doi:10.1128/mcb.00171-22.
14. Childs BG, Gluscevic M, Baker DJ, Laberge RM, Marquess D, Dananberg J, van Deursen JM. Senescent cells: an emerging target for diseases of ageing. Nat Rev Drug Discov. 2017;16(10):718–735. doi:10.1038/nrd.2017.116.
15. Yoshida S, Nakagami H, Hayashi H, Ikeda Y, Sun J, Tenma A, Tomioka H, Kawano T, Shimamura M, Morishita R, et al. The CD153 vaccine is a senotherapeutic option for preventing the accumulation of senescent T cells in mice. Nat Commun. 2020;11(1):2482. doi:10.1038/s41467-020-16347-w.
16. Amor C, Feucht J, Leibold J, Ho YJ, Zhu C, Alonso-Curbelo D, Mansilla-Soto J, Boyer JA, Li X, Giavridis T, et al. Senolytic CAR T cells reverse senescence-associated pathologies. Nature. 2020;583(7814):127–132. doi:10.1038/s41586-020-2403-9.
17. Das A, Ali N. Nanovaccine: an emerging strategy. Expert Rev Vaccines. 2021;20(10):1273–1290. doi:10.1080/14760584.2021.1984890.

18. Wen R, Umeano AC, Kou Y, Xu J, Farooqi AA. Nanoparticle systems for cancer vaccine. Nanomed (Lond). 2019;14 (5):627–648. doi:10.2217/nnm-2018-0147.
19. Wilson JT. A sweeter approach to vaccine design. Science. 2019;363(6427):584–585. doi:10.1126/science.aav9000.
20. Zhang J, Fan J, Skwarczynski M, Stephenson RJ, Toth I, Hussein WM. Peptide-based nanovaccines in the treatment of cervical cancer: a review of recent advances. Int J Nanomed. 2022;17:869–900. doi:10.2147/IJN.S269986.
21. Jiang J. Cell-penetrating peptide-mediated nanovaccine delivery. Curr Drug Targets. 2021;22(8):896–912. doi:10.2174/1389450122666210203193225.
22. Xu F, Yuan Y, Wang Y, Yin Q. Emerging peptide-based nanovaccines: from design synthesis to defense against cancer and infection. Biomed Pharmacother. 2023;158:114117. doi:10.1016/j.biopha.2022.114117.
23. Abdelwahab WM, Auclair S, Borgogna T, Siram K, Riffey A, Bazin HG, Cottam HB, Hayashi T, Evans JT, Burkhart DJ. Co-delivery of a novel lipidated TLR7/8 agonist and hemagglutinin-based influenza antigen using silica nanoparticles promotes enhanced immune responses. Pharmaceutics. 2024, 16. 16(1):107. doi:10.3390/pharmaceutics16010107.
24. Zhang L, Ma C, Sun J, Shao B, Portale G, Chen D, Liu K, Herrmann A. Genetically engineered supercharged polypeptide fluids: fast and persistent self-ordering induced by touch. Angew Chem Int Ed Engl. 2018;57(23):6878–6882. doi:10.1002/anie.201803169.
25. Ma C, Li B, Zhang J, Sun Y, Li J, Zhou H, Shen J, Gu R, Qian J, Fan C, et al. Significantly improving the bioefficacy for rheumatoid arthritis with supramolecular nanoformulations. Adv Mater. 2021;33(16):e2100098. doi:10.1002/adma.202100098.
26. Li J, Li B, Sun J, Ma C, Wan S, Li Y, Gostl R, Herrmann A, Liu K, Zhang H. Engineered near-infrared fluorescent protein assemblies for robust bioimaging and therapeutic applications. Adv Mater. 2020;32(17):e2000964. doi:10.1002/adma.202000964.
27. Mendelsohn AR, Larrick JW. Antiaging vaccines targeting senescent cells. Rejuvenation Res. 2022;25(1):39–45. doi:10.1089/rej.2022.0008.
28. Gong N, Ma X, Ye X, Zhou Q, Chen X, Tan X, Yao S, Huo S, Zhang T, Chen S, et al. Carbon-dot-supported atomically dispersed gold as a mitochondrial oxidative stress amplifier for cancer treatment. Nat Nanotechnol. 2019;14(4):379–387. doi:10.1038/s41565-019-0373-6.
29. Dienz O, Rincon M. The effects of IL-6 on CD4 T cell responses. Clin Immunol. 2009;130(1):27–33. doi:10.1016/j.clim.2008.08.018.
30. Lanzavecchia A, Sallusto F. Regulation of T cell immunity by dendritic cells. Cell. 2001;106(3):263–266. doi:10.1016/s0092-8674(01)00455-x.
31. Prabata A, Ikeda K, Rahardini EP, Hirata KI, Emoto N. GPNMB plays a protective role against obesity-related metabolic disorders by reducing macrophage inflammatory capacity. J Biol Chem. 2021;297(5):101232. doi:10.1016/j.jbc.2021.101232.
32. Nickl B, Qadri F, Bader M. Anti-inflammatory role of Gpnmb in adipose tissue of mice. Sci Rep. 2021;11(1):19614. doi:10.1038/s41598-021-99090-6.
33. Ribeiro R, Macedo JC, Costa M, Ustiyan V, Shindyapina AV, Tyshkovskiy A, Gomes RN, Castro JP, Kalin TV, Vasques-Nóvoa F, et al. In vivo cyclic induction of the FOXM1 transcription factor delays natural and progeroid aging phenotypes and extends healthspan. Nat Aging. 2022;2 (5):397–411. doi:10.1038/s43587-022-00209-9.
34. Hwang HJ, Kim N, Herman AB, Gorospe M, Lee JS. Factors and pathways modulating endothelial cell senescence in vascular aging. Int J Mol Sci. 2022; 23(17):10135. doi:10.3390/ijms231710135.
35. Suda M, Shimizu I, Katsuumi G, Hsiao CL, Yoshida Y, Matsumoto N, Yoshida Y, Katayama A, Wada J, Seki M, et al. Glycoprotein nonmetastatic melanoma protein B regulates lysosomal integrity and lifespan of senescent cells. Sci Rep. 2022;12 (1):6522. doi:10.1038/s41598-022-10522-3.
36. Diaz-Ortiz ME, Seo Y, Posavi M, Carceles Cordon M, Clark E, Jain N, Charan R, Gallagher MD, Unger TL, Amari N, et al. GPNMB confers risk for Parkinson's disease through interaction with α-synuclein. Science. 2022;377(6608):eabk0637. doi:10.1126/science.abk0637.
37. Saade M, Araujo de Souza G, Scavone C, Kinoshita PF. The role of GPNMB in inflammation. Front Immunol. 2021;12:674739. doi:10.3389/fimmu.2021.674739.
38. Qin L, Zhang H, Zhou Y, Umeshappa CS, Gao H. Nanovaccine-based strategies to overcome challenges in the whole vaccination cascade for tumor immunotherapy. Small. 2021;17(28):e2006000. doi:10.1002/smll.202006000.
39. Koirala P, Bashiri S, Toth I, Skwarczynski M. Current prospects in peptide-based subunit nanovaccines. Methods Mol Biol. 2022;2412:309–338. doi: 10.1007/978-1-0716-1892-9_16. doi:10.1007/978-1-0716-1892-9_16.
40. Huang W, Madge HYR, Zhang J, Gilmartin L, Hussein WM, Khalil ZG, Koirala P, Capon RJ, Toth I, Stephenson RJ. Structure-activity relationship of lipid, cyclic peptide and antigen rearrangement of physically mixed vaccines. Int J Pharm. 2022;617:121614. doi:10.1016/j.ijpharm.2022.121614.
41. Zumerle S, Sarill M, Saponaro M, Colucci M, Contu L, Lazzarini E, Sartori R, Pezzini C, Rinaldi A, Scanu A, et al. Targeting senescence induced by age or chemotherapy with a polyphenol-rich natural extract improves longevity and healthspan in mice. Nat Aging. 2024;4(9):1231–1248. doi:10.1038/s43587-024-00663-7.
42. Chaib S, Tchkonia T, Kirkland JL. Cellular senescence and senolytics: the path to the clinic. Nat Med. 2022;28(8):1556–1568. doi:10.1038/s41591-022-01923-y.
43. Carmona-Ribeiro AM, Perez-Betancourt Y. Cationic nanostructures for vaccines design. Biomim (Basel). 2020;5(3):5. doi:10.3390/biomimetics5030032.
44. Heuts J, Jiskoot W, Ossendorp F, van der Maaden K. Cationic nanoparticle-based cancer vaccines. Pharmaceutics. 2021 13. 13 (5):596. doi:10.3390/pharmaceutics13050596.
45. Lam N, Lee Y, Farber DL. A guide to adaptive immune memory. Nat Rev Immunol. 2024;24(11):810–829. doi:10.1038/s41577-024-01040-6.
46. Dominguez-Andres J, Dos Santos JC, Bekkering S, Mulder WJM, van der Meer JWM, Riksen NP, Joosten LAB, Netea MG. Trained immunity: adaptation within innate immune mechanisms. Physiol Rev. 2023;103(1):313–346. doi:10.1152/physrev.00031.2021.
47. Wang TW, Johmura Y, Suzuki N, Omori S, Migita T, Yamaguchi K, Hatakeyama S, Yamazaki S, Shimizu E, Imoto S, et al. Blocking PD-L1–PD-1 improves senescence surveillance and ageing phenotypes. Nature. 2022;611(7935):358–364. doi:10.1038/s41586-022-05388-4.
48. Xu Q, Fu Q, Li Z, Liu H, Wang Y, Lin X, He R, Zhang X, Ju Z, Campisi J, et al. The flavonoid procyanidin C1 has senotherapeutic activity and increases lifespan in mice. Nat Metab. 2021;3 (12):1706–1726. doi:10.1038/s42255-021-00491-8.